NANO LETTERS

pubs.acs.org/NanoLett Letter

Phase Transition Photodetection in Charge Density Wave Tantalum Disulfide

Chunhe Dang, Mengxue Guan, Sabir Hussain, Wen Wen, Yiming Zhu, Liying Jiao, Sheng Meng, and Liming Xie*

Cite This: *Nano Lett.* 2020, 20, 6725−6731 Read Online

ACCESS | Metrics & More | Article Recommendations | Supporting Information

ABSTRACT: The charge density wave (CDW) phase is a macroscopic quantum state with periodic charge density modulation accompanied by periodic lattice distortion in low-dimensional metals. External fields, such as an electric field and optical excitation, can trigger the transitions among different CDW states, leaving an under-explored mechanism and attracting great interest toward optoelectronic applications. Here, we explore a photo-induced phase transition in 1T-TaS_2 under an electrical field. By analyzing the phase transition probability, we obtained a linear dependence of the phase transition barrier on the electric field and laser energy density. Additionally, the threshold laser energy for the phase transition decreases linearly with an increasing applied electrical field. Finally, picojoule photodetection was realized in the visible and near-infrared ranges near the CDW transition edge. Our work will promote the understanding of the CDW phase transition mechanism as well as open pathways for optoelectronic applications.

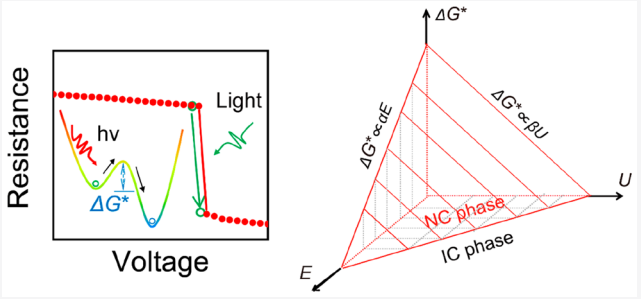

KEYWORDS: *phase transition, 1T-TaS_2, charge density wave, energy barrier, photodetection*

The charge density wave (CDW) is a symmetry-broken state with a band gap opening caused by electron−phonon or electron−electron interactions in metals.[1,2] Different from ordinary metals where only single-particle excitation exists, there are collective excitations in the CDW systems,[1,2] which hold great potential for electronic and optoelectronic applications,[3−12] such as high-energy radiation-immune and nontransistor electronics,[7−10] photodetectors,[11,12] and so on. Layered transition metal dichalcogenide tantalum disulfide (1T-TaS_2) undergoes different CDW orders by decreasing the temperature, which are various equilibrium states with energy barriers among them.[5] External perturbation, such as electric fields and light stimulation, can drive the phase transitions among various CDW states,[4,6,13−22] leaving the debate about whether the mechanism of self-heating is negligible or not.[10,17,23−26] Although phase transition under both electric field and light[12,26] was investigated in 1T-TaS_2, more quantitative information is highly needed.

Phase transitions with a steep resistance change hold great potential for photodetection, for example, superconductor−normal metal transition for single-photon detection,[27−29] insulator−metal transition in VO_2 for highly sensitive thermal irradiation detection,[30,31] and so on. In the phase-transition-based photodetection, the device temperature is set near the phase transition temperature, in which photon absorption can greatly change the resistance of the materials, and hence it shows ultrahigh photosensitivity. The electrically driven CDW phase transition at room temperature in 1T-TaS_2 with a sharp transition edge[6,32] is also promising for ultrasensitive uncooled photodetection.[12]

In this report, we investigated an optical-pulse-triggered nearly commensurate CDW (NCCDW) to incommensurate CDW (ICCDW) phase transition in 1T-TaS_2 near the electric-field-driven phase transition edge. Measurement of the phase transition probability under an electric field and light illumination reveals a linear dependence of the phase transition energy barrier on the electric field and laser energy density. The slope of the phase transition barrier to the photon flux density at a laser wavelength of 532 nm was 5 times steeper than that at 1064 nm, which indicates a wavelength-dependent photoinduced phase transition mechanism. Finally, by setting the bias voltage close to the phase transition edge, picojoule photodetection in visible and near-infrared ranges was achieved in this CDW transition edge photodetector.

Figure 1a shows the structure of the 1T-TaS_2 layer, which consists of a Ta layer sandwiched between two S layers, and each Ta atom is coordinated octahedrally by six S atoms.[33,34]

Received: June 23, 2020
Revised: August 5, 2020
Published: August 5, 2020

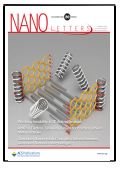

https://dx.doi.org/10.1021/acs.nanolett.0c02613
Nano Lett. 2020, 20, 6725−6731

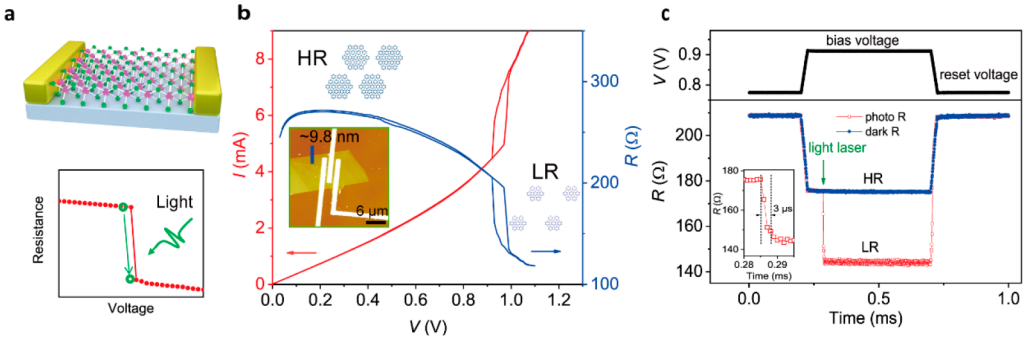

Figure 1. Optical-pulse-induced CDW transitions near the transition edge in 1T-TaS_2. (a) Device structure of 1T-TaS_2 and schematic illustration of photodetection near the CDW transition edge. (b) Electrically driven phase transition between NCCDW and ICCDW states. Inset: Microscopic structure of the high-resistance (HR) NCCDW state and the low-resistance (LR) ICCDW state. The middle inset image is an atomic force microscopy image of the device, showing a thickness of 9.8 nm. (c) Photodetection near the transition edge under a 532 nm pulsed laser (pulse width of 1.3 ns, pulse energy of 0.216 pJ/μm^2, 1 kHz repetition rate). Top panel: Voltage waveform. Bottom panel: Resistance curves with and without pulsed light illumination. Inset: Zoomed-in curve near the resistance drop.

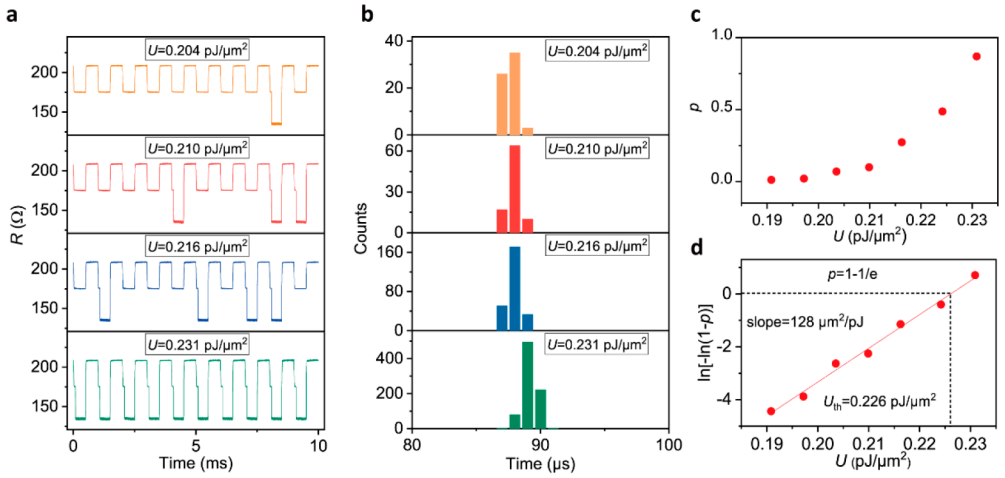

Figure 2. Laser-energy-density-dependent CDW phase transitions at an electric field of 13.8 kV/cm. (a) Photoinduced phase transitions when applying laser pulses (532 nm, pulse width of 1.3 ns) of different energy densities (U). The resistance change down to <150 Ω was from photoinduced phase transitions. (b) Counts of the waveforms with phase transitions (N = 941, 939, 936, and 921 from top to bottom). The photoinduced phase transition occurred at around 90 μs. (c) Plot of phase transition probability (p) against energy density (U) of the applied laser pulse. (d) Linear fitting of $\ln[-\ln(1-p)]$ to U. The energy density at $\ln[-\ln(1-p)] = 0$ (i.e., $p = 1 - 1/e$) is defined as the threshold laser energy density U_{th}.

Figure 1b shows a typical $I-V$ characteristic of 1T-TaS_2, which displays the electrically induced phase transition from the NCCDW to the ICCDW state with a sharp decrease of the resistance of about 30% at a threshold voltage, V_H, of 970 mV (corresponding to an electric field of ~14.7 kV/cm). When the voltage swept back, the LR state recovered with a lower threshold voltage, V_L, of 920 mV; that is, there was a hysteresis window.

When a bias voltage of 911 mV was set below the threshold voltage (V_H = 923 mV; note that the threshold voltage shifted in comparison to that in the static $I-V$ sweep shown in Figure 1b), there was no resistance change under dark conditions (the blue curve in Figure 1c). After a laser pulse was applied (532 nm, 1.3 ns pulse, energy density of 0.216 pJ/μm^2), a resistance jump from 175 to 142 Ω was observed at the time when the laser pulse was applied (the red curve in Figure 1c). This energy density (sub pJ/μm^2) for triggering the CDW phase transition under an electric field in 1T-TaS_2 is much lower than that needed for the CDW phase transition without an electric field (~10 pJ/μm^2).[17,25]

Due to the hysteresis of the phase transition, the device could not recover to the HR state after the light pulse was removed. A reset voltage of 776 mV (lower than V_L of 895 mV) was applied to reset the device to the initial HR state. The single-pulse-triggered resistance falling time was about 3 μs (see inset of Figure 1c), several orders longer than the reported time scale (femtoseconds to nanoseconds) for photoinduced CDW phase transitions without an electric field in 1T-TaS_2.[17,35,36] This resistance falling time is at the same time scale as that observed in 1T-TaS_2-based oscillators.[6,10] A possible explanation is that the phase transition was initiated at a point location in which a longer time (time scale of microseconds or more) was needed for the avalanche process to form a LR conducting channel, similar to that in electrically driven insulator−metal phase transition in VO_2.[37,38]

The phase transition probability, defined as the waveforms with phase transitions divided by the total sampled waveforms, changed with the light energy density (Figure 2a). As the energy density of the laser pulse increased from 0.204 to 0.231 pJ/μm^2, the photoinduced phase transition probability increased nonlinearly from 0.069 to 0.869 (Figure 2a−c).

https://dx.doi.org/10.1021/acs.nanolett.0c02613
Nano Lett. 2020, 20, 6725−6731

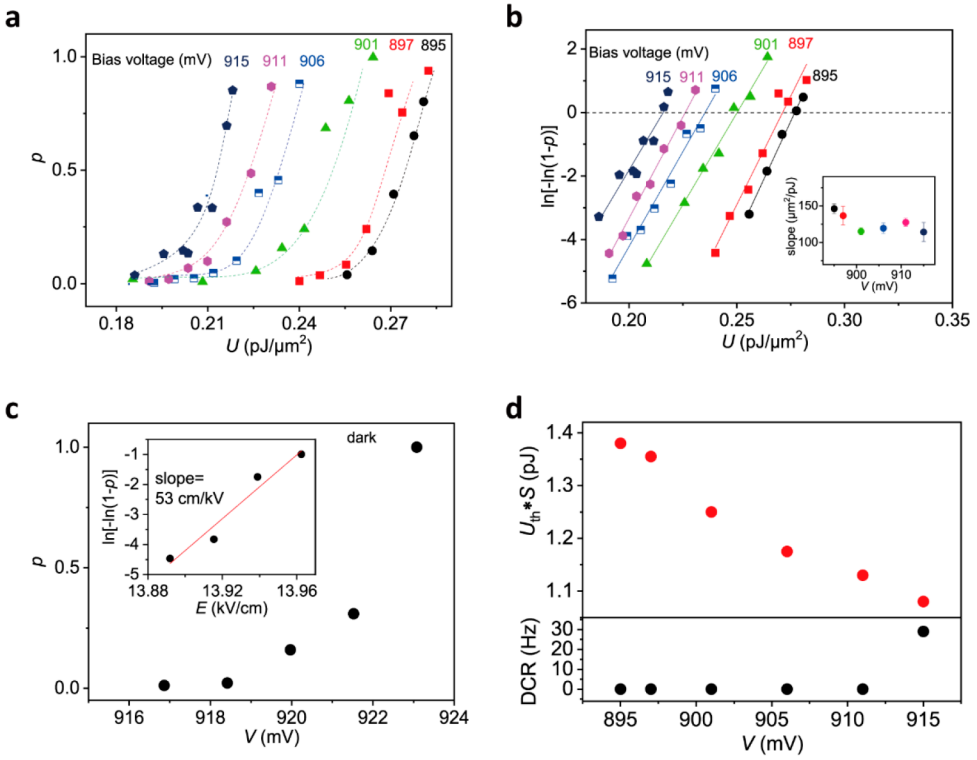

Figure 3. Photodetection at different bias voltages under 532 nm light pulses. (a) Plot of phase transition probability (p) against energy density of the laser pulse (U) at various bias voltages. Dashed colored lines are guides for the eyes. (b) Linear fitting of $\ln[-\ln(1-p)]$ versus U at different bias voltages. Inset: Fitted slopes at different bias voltages. (c) Phase transition probability in dark condition. Inset: $\ln[-\ln(1-p)]$ can be fitted linearly with the electric field in dark conditions. (d) Threshold laser energy U_{th}*S and phase transition dark count rate (DCR) at different bias voltage. S is the channel area of the device (~5 μm^2 for this device).

The phase transition always occurred at the time when the laser pulses were applied (Figure 2b), confirming that all of these phase transitions were triggered by the laser pulses.

Considering the finite width (1.3 ns) of the laser pulse and the irreversibility of the phase transition during one single pulse duration, the observed phase transition probability, p, was not proportional to the average phase transition probability per unit of time. If the phase transition was reversible, multiple phase transitions would occur and the phase transition events within a single laser pulse duration would obey Poisson distribution. Further analysis (see Supporting Information Figure S1) shows that the zero-phase transition probability, $1-p$, is related to the phase transition energy barrier ΔG^*:

$$\ln[-\ln(1-p)] = A - \Delta G^*/k_B T \quad (1)$$

where A is a constant, k_B is the Boltzmann constant, and T is the temperature in kelvin (T = 300 K).

The experimentally observed dependence of $\ln[-\ln(1-p)]$ on the light energy density U showed a linear behavior (Figure 2d). This indicates that the phase transition energy barrier decreases linearly with the increasing energy density of the laser pulse. The fitted slope for $\ln[-\ln(1-p)]$ on U was 128 μm^2/pJ, corresponding to an energy barrier decrease of 128 $k_B T$ per pJ/μm^2 of light energy. Further, a threshold laser energy density, U_{th}, was defined as the laser energy at $\ln[-\ln(1-p)] = 0$ (i.e., $p = 1 - 1/e$). For the device shown in Figure 2, the U_{th} was 0.226 pJ/μm^2 under an applied voltage of 911 mV (V_H of 923 mV).

The experimentally observed linear dependence of the energy barrier as a function of laser energy density is consistent with a recent calculation for the mechanism of the photodriven CDW phase transition in 1T-TaS_2. In the calculation, light generates charge carriers in 1T-TaS_2, and the energy difference between the two phases is decreases linearly to the photon density.[25] We also calculated the energy difference between the CCDW phase and normal metal phases of 1T-TaS_2 under light excitation at E = 0 (see Supporting Information Figure S2). Calculation showed that, without an electric field, the energy difference between the CCDW state and the normal metal state of 1T-TaS_2 decreased as light energy density increased. In a narrow range of light energy, the energy difference changes quasi-linearly to the light energy.

The photoinduced phase transition probability was also measured at different bias voltages (Figure 3). The phase transition probabilities against the energy density of the laser pulse showed similar behavior at different bias voltages: p increased nonlinearly with increasing U (Figure 3a) and $\ln[-\ln(1-p)]$ changed linearly with similar slopes (127 ± 12 μm^2/pJ, Figure 3b). This indicates that the phase transition energy barrier changes similarly with the energy density of the laser pulse at different electric fields.

The phase transition probability in dark conditions increased as the bias voltage increased (Figure 3c). The phase transition under dark conditions, which was a spontaneous process, occurred at random time positions as expected (Supporting Information Figure S3). The $\ln[-\ln(1-p)]$ against the applied voltage under dark conditions can be fitted linearly, yielding a slope of 53 cm/kV. This slope suggests that the phase transition energy barrier changes linearly to the electric field with a coefficient of 53 $k_B T$ per kV/cm.

https://dx.doi.org/10.1021/acs.nanolett.0c02613
Nano Lett. 2020, 20, 6725−6731

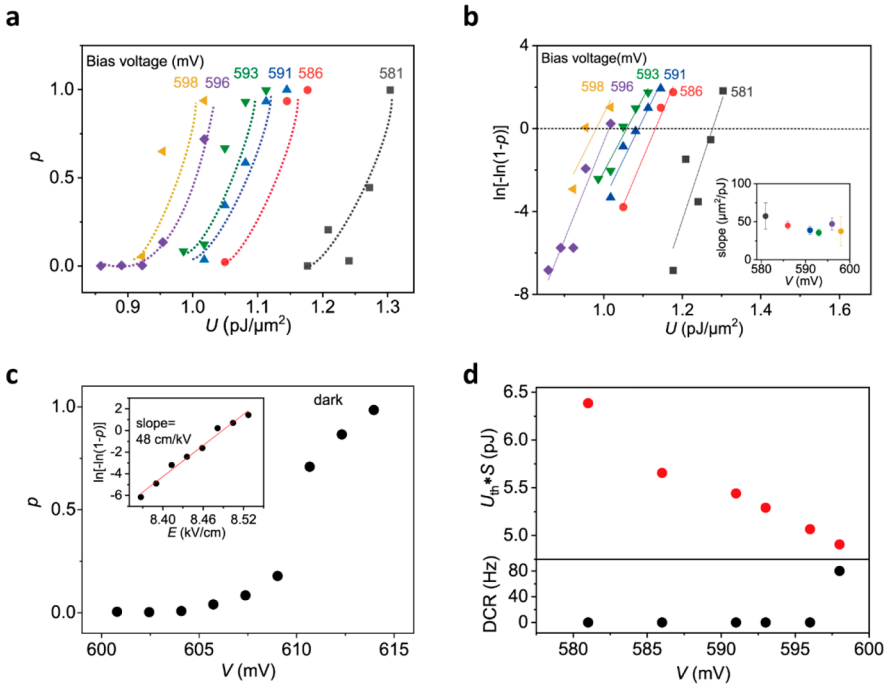

Figure 4. Photodetection near the CDW phase transition edge under 1064 nm light pulses. (a) Phase transition probability p versus laser energy density U (1064 nm, 1.3 ns) at various bias voltages for a 1T-TaS_2 device with V_H of 615 mV (see device information in Supporting Information Figure S4). Colored dashed lines are guides for the eyes. (b) Linear fitting of $\ln[-\ln(1-p)]$ versus U at different bias voltages. Inset: Slopes of the fitted lines at different bias voltages. (c) Voltage-dependent phase transition probability under dark conditions. Inset: Linear fitting of $\ln[-\ln(1-p)]$ to the electric field. (d) Voltage-dependent threshold laser energy and phase transition dark count rate.

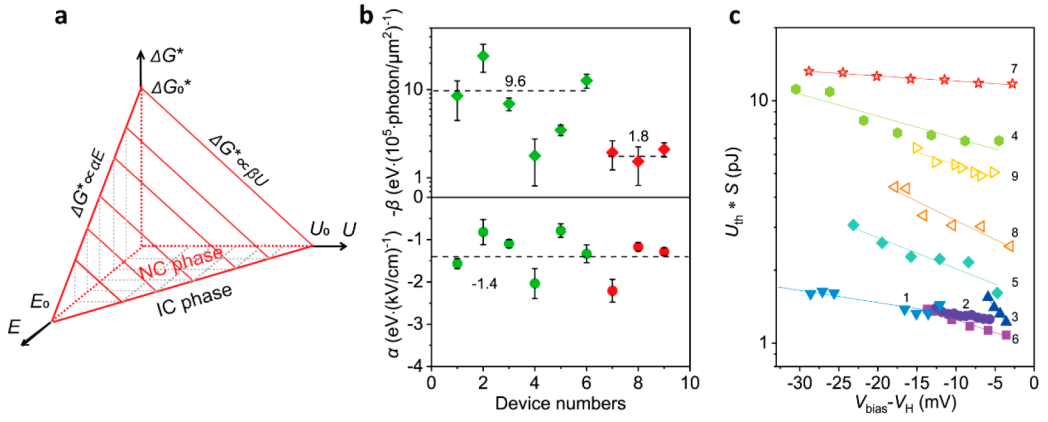

Figure 5. Comparison of picojoule photodetection at laser wavelengths of 532 and 1064 nm. (a) Illustration of the phase transition energy barrier in 1T-TaS_2 under an electric field and light energy density. (b) Plot of slopes α and β indicated in (a) for different devices. (c) Threshold light energy density versus the bias voltage (V_{bias}) from the threshold voltage V_H. Device # is labeled next to the data point. In panels (b,c), device #1−6 and 7−9 were measured under 532 and 1064 nm illumination, respectively.

The threshold laser energy to achieve a phase transition probability of $p = 1 - 1/e$, which is equal to $U_{th}*S$ (S is the device area), is used as the photosensitivity parameter of the devices (Figure 3d, top panel). As the applied voltage increased from 895 to 915 mV, $U_{th}*S$ decreased from ∼1.4 to ∼1.1 pJ; that is, less light energy was needed to drive the phase transition as the bias voltage was closer to the CDW phase transition edge. At the bias voltage of 915 mV (8 mV from the V_H of 923 mV), the photosensitivity of this CDW phase transition photodetector was about 1.1 pJ. The phase transition dark count rate was about 29 Hz at the bias voltage of 915 mV (Figure 3d, bottom panel).

The photoinduced phase transition near the transition edge of 1T-TaS_2 was also investigated under NIR laser pulses (1064 nm, pulse width of 1.3 ns). The phase transition behavior was similar to that observed under 532 nm laser pulses. The transition probability p increased nonlinearly as the energy density of the laser pulse (Figure 4a) and the fitting of $\ln[-\ln(1-p)]$ to the energy density were linear with similar slopes (44 ± 8 μm^2/pJ) (Figure 4b). The phase transition probability under dark conditions increased from 0.004 to 0.984 when the bias voltage increased from 601 to 614 mV (Figure 4c). The threshold laser energy, $U_{th}*S$, decreased with increasing the electric field (see Figure 4d), reaching 4.9 pJ at 598 mV (about 17 mV from V_H of 615 mV). The phase transition dark count rate was about 80 Hz at 598 mV.

The phase transition probability measurement reveals a linear dependence of the phase transition energy barrier to the

https://dx.doi.org/10.1021/acs.nanolett.0c02613
Nano Lett. 2020, 20, 6725−6731

electric field and the light energy density. No obvious cross-correlation is observed between the electric field and light illumination. Then the phase transition barrier, ΔG^*, as a function of the electric field, E, and the light energy density, U, can be plotted, which is a plane (Figure 5a) in the $E-U-\Delta G^*$ space. The slope of ΔG^*-E in the plane of $U = 0$ is denoted as α. The slope α is the energy barrier change coefficient to the electric field and is measured from the phase transition probability in dark conditions. The slope of ΔG^*-U in the plane with a fixed E is denoted as β. The slope β is the energy barrier change coefficient to the light energy density and measured from the phase transition probability under light illumination at the electric field E. Experiments on more devices give an average α value of -1.4 ± 0.5 eV·(kV/cm)$^{-1}$ (Figure 5b, bottom panel). The measured β values were -2.6 ± 2.2 and -0.98 ± 0.14 eV·(pJ/μm^2)$^{-1}$ [corresponding to -9.6 ± 8.1 and -1.8 ± 0.3 eV·(10^5 photon/μm^2)$^{-1}$], at 532 and 1064 nm light illuminations, respectively (Figure 5b, top panel).

According to the mechanisms of the photoinduced CDW phase transition without an electric field in 1T-TaS_2, the photons excite electrons to the conduction band and stabilize the normal metal state.[25] Based on this, the phase transition barrier should be proportional to the photon density without light wavelength dependence.[24] However, the ΔG^*-U slope (i.e., the β coefficient) at 532 nm is 5 times steeper than that at 1064 nm. This indicates that the energy barrier decreases faster at 532 nm illumination, and hence a wavelength-dependent photoinduced phase transition mechanism near the CDW transition edge should be expected. Considering the high electric field (~10 kV/cm) near the electrically driven phase transition edge, there may be carrier multiplication.[13] For short wavelength (532 nm) light irradiation, the high-energy photon-excited electrons in the conduction band may lead to more carrier multiplication under an electric field, resulting in a larger change coefficient of the energy barrier.

The photosensitivity for different devices is shown in Figure 5c. The photosensitivity of different devices varies from 1.1 to 12 pJ. As the bias voltage increases close to the CDW transition edge, V_H, the threshold laser energy density decreases almost linearly. The best device in our experiments shows a photosensitivity of 1.1 pJ at 4 mV from the transition edge under 532 nm illumination and 2.5 pJ at 3 mV from the transition edge under 1064 nm illumination. Considering that the electrically driven phase transition in Mott insulators is usually triggered at a point location,[38] the actual light power needed to trigger the phase transition in 1T-TaS_2 should be much lower.

To summarize, we have investigated the photoinduced CDW phase transition behavior near the electrically driven NCCDW–ICCDW transition edge in 1T-TaS_2. The phase transition energy barrier was revealed to be linear to the electric field and the light energy density. The slope of the phase transition barrier to the photon flux density at a laser wavelength of 532 nm was 5 times steeper than that at 1064 nm, which indicates more multiplication of the photoinduced carriers for high-energy photons near the CDW transition edge. The CDW-based photodetector near the phase transition edge was demonstrated. At the bias voltage of a few millivolts away from the transition edge, picojoule photodetection was achieved in visible and near-infrared ranges. Closer approach of the bias voltage to the CDW transition edge could further enhance the photosensitivity. Though far from optimized, our findings greatly promote the understanding on the CDW phase transition mechanism in tantalum disulfide under external fields and sheds new light on uncooled ultrasensitive photodetectors.

METHODS

Device Fabrication. High-quality 1T-TaS_2 thin flakes (~20 nm) were obtained by mechanical exfoliation from the bulk single crystals onto a SiO_2/Si (300 nm oxide) wafer in a glovebox. Optical contrast (Olympus BX53) was used to identify the thin flakes. Metal electrodes (Cr/Au, 8 nm/80 nm) were patterned using a standard electron-beam lithography process and deposited by an electronic beam evaporation. To protect the sample from oxidation, air exposure was minimized during the fabrication process. Atomic force microscopy (AFM) imaging was performed on a commercial AFM system (MFP-3D Infinity, Asylum Research) in the atmospheric circumstance with the tapping mode.

Optoelectronic Measurement. The measurement was performed in the vacuum chamber of a Lakeshore probe station (Lakeshore TTP4). The static $I-V$ characteristics were obtained by a semiconductor parameter analyzer (Keithley 4200-SCS, Tektronix). The electric voltage pulses were supplied by an arbitrary function generator (AFG 1062, Tektronix Inc.), and the data were collected by a digit multimeter (DMM 7510, Tektronix). We used trapezoid-wave voltage pulses with 25 μs rise time (channel 1) at a frequency of 1 kHz on 1T-TaS_2 devices. Another 1 kHz square-wave voltage pulse (channel 2) was used to trigger pulse lasers at the same frequency. For the optical measurements, a 514 nm pulsed laser with pulse width of 1.3 ns (product# MPL-III-532, Changchun New Industries Optoelectronics Tech. Co., Ltd., China) and a 1064 nm pulsed laser with pulse width of 1.3 ns (MPL-III-1064, Changchun New Industries Optoelectronics Tech. Co., Ltd., China) were introduced into the probe station for light illumination on 1T-TaS_2 devices. Tunable neutral density filters (NDC-50C-4M-A for 532 nm laser, NDC-50C-4 M for 1064 nm laser, Thorlabs) were used to tune the laser power on the devices.

ASSOCIATED CONTENT

Supporting Information

The Supporting Information is available free of charge at https://pubs.acs.org/doi/10.1021/acs.nanolett.0c02613.

Analysis of the energy barrier as a function of the phase transition probability; calculated energy barrier at different laser fluences; comparison of the phase transition under dark conditions and under laser illumination; AFM image and electrical characteristics of the 1T-TaS_2 device (PDF)

AUTHOR INFORMATION

Corresponding Author

Liming Xie – *CAS Key Laboratory of Standardization and Measurement for Nanotechnology, CAS Center for Excellence in Nanoscience, National Center for Nanoscience and Technology, Beijing 100190, P.R. China; University of Chinese Academy of Sciences, Beijing 100049, P.R. China;* orcid.org/0000-0001-8190-8325; Email: xielm@nanoctr.cn

https://dx.doi.org/10.1021/acs.nanolett.0c02613
Nano Lett. 2020, 20, 6725–6731

Authors

Chunhe Dang − *CAS Key Laboratory of Standardization and Measurement for Nanotechnology, CAS Center for Excellence in Nanoscience, National Center for Nanoscience and Technology, Beijing 100190, P.R. China; University of Chinese Academy of Sciences, Beijing 100049, P.R. China; Department of Chemistry, Tsinghua University, Beijing 100084, P.R. China*

Mengxue Guan − *Beijing National Laboratory for Condensed Matter Physics, Institute of Physics, Chinese Academy of Sciences, Beijing 100190, P.R. China;* orcid.org/0000-0002-6987-4211

Sabir Hussain − *CAS Key Laboratory of Standardization and Measurement for Nanotechnology, CAS Center for Excellence in Nanoscience, National Center for Nanoscience and Technology, Beijing 100190, P.R. China; University of Chinese Academy of Sciences, Beijing 100049, P.R. China;* orcid.org/0000-0002-9259-5376

Wen Wen − *CAS Key Laboratory of Standardization and Measurement for Nanotechnology, CAS Center for Excellence in Nanoscience, National Center for Nanoscience and Technology, Beijing 100190, P.R. China; University of Chinese Academy of Sciences, Beijing 100049, P.R. China*

Yiming Zhu − *CAS Key Laboratory of Standardization and Measurement for Nanotechnology, CAS Center for Excellence in Nanoscience, National Center for Nanoscience and Technology, Beijing 100190, P.R. China*

Liying Jiao − *Department of Chemistry, Tsinghua University, Beijing 100084, P.R. China;* orcid.org/0000-0002-6576-906X

Sheng Meng − *Beijing National Laboratory for Condensed Matter Physics, Institute of Physics, Chinese Academy of Sciences, Beijing 100190, P.R. China;* orcid.org/0000-0002-1553-1432

Complete contact information is available at: https://pubs.acs.org/10.1021/acs.nanolett.0c02613

Author Contributions

L.X. conceived the project. C.D. fabricated 1T-TaS_2 thin film devices and performed electric and optical measurements. W.W. and Y.Z. advised the fabrication process. M.G. and S.M. did the time-dependent density functional theory calculation. S.H. performed the AFM imaging. L.J. advised the manuscript preparation. C.D. and L.X. wrote the paper, and all authors commented on the manuscript.

Notes

The authors declare no competing financial interest.

■ ACKNOWLEDGMENTS

L.X. acknowledges support from NSFC (21673058, 21822502), the Key Research Program of Frontier Sciences of CAS (QYZDB-SSW-SYS031), and the Strategic Priority Research Program of CAS (XDB30000000).

■ REFERENCES

(1) Grüner, G. *Density Waves in Solids*; Perseus: Cambridge, MA 2000.

(2) Grüner, G. The Dynamics of Charge Density Waves. *Phys. Scr.* **1985**, *32*, 11−25.

(3) Ogawa, N.; Miyano, K. Charge-density wave as an electro-optical switch and memory. *Appl. Phys. Lett.* **2002**, *80*, 3225−3227.

(4) Vaskivskyi, I. Fast electronic resistance switching involving hidden charge density wave states. *Nat. Commun.* **2016**, *7*, 11442.

(5) Yoshida, M.; Suzuki, R.; Zhang, Y.; Nakano, M.; Iwasa, Y. Memristive phase switching in two-dimensional 1T-TaS_2 crystals. *Sci. Adv.* **2015**, *1*, No. e1500606.

(6) Liu, G.; et al. A charge-density-wave oscillator based on an integrated tantalum disulfide−boron nitride−graphene device operating at room temperature. *Nat. Nanotechnol.* **2016**, *11*, 845−850.

(7) Khitun, A.; Liu, G.; Balandin, A. A. Two-Dimensional Oscillatory Neural Network Based on Room-Temperature Charge-Density-Wave Devices. *IEEE Trans. Nanotechnol.* **2017**, *16*, 860−867.

(8) Khitun, A. G.; Geremew, A. K.; Balandin, A. A. Transistor-Less Logic Circuits Implemented With 2-D Charge Density Wave Devices. *IEEE Electron Device Lett.* **2018**, *39*, 1449−1452.

(9) Geremew, A. K.; et al. Proton-irradiation-immune electronics implemented with two-dimensional charge-density-wave devices. *Nanoscale* **2019**, *11*, 8380−8386.

(10) Wen, W.; Zhu, Y.; Dang, C.; Chen, W.; Xie, L. Raman Spectroscopic and Dynamic Electrical Investigation of Multi-State Charge-Wave-Density Phase Transitions in 1*T*-TaS_2. *Nano Lett.* **2019**, *19*, 1805−1813.

(11) Wang, L.; et al. Distinctive Performance of Terahertz Photodetection Driven by Charge-Density-Wave Order in CVD-Grown Tantalum Diselenide. *Adv. Funct. Mater.* **2019**, *29*, 1905057.

(12) Wu, D.; et al. Ultrabroadband photosensitivity from visible to terahertz at room temperature. *Sci. Adv.* **2018**, *4*, No. eaao3057.

(13) Hollander, M. J.; et al. Electrically Driven Reversible Insulator−Metal Phase Transition in 1T-TaS_2. *Nano Lett.* **2015**, *15*, 1861−1866.

(14) Yu, Y.; et al. Gate-tunable phase transitions in thin flakes of 1T-TaS_2. *Nat. Nanotechnol.* **2015**, *10*, 270−276.

(15) Ma, L. A metallic mosaic phase and the origin of Mott-insulating state in 1T-TaS_2. *Nat. Commun.* **2016**, *7*, 10956.

(16) Cho, D. Nanoscale manipulation of the Mott insulating state coupled to charge order in 1T-TaS_2. *Nat. Commun.* **2016**, *7*, 10453.

(17) Stojchevska, L.; et al. Ultrafast Switching to a Stable Hidden Quantum State in an Electronic Crystal. *Science* **2014**, *344*, 177−180.

(18) Hellmann, S. Ultrafast Melting of a Charge-Density Wave in the Mott Insulator 1T-TaS_2. *Phys. Rev. Lett.* **2010**, *105*, 187401.

(19) Eichberger, M.; et al. Snapshots of cooperative atomic motions in the optical suppression of charge density waves. *Nature* **2010**, *468*, 799−802.

(20) Laulhé, C. Ultrafast Formation of a Charge Density Wave State in 1T-TaS_2: Observation at Nanometer Scales Using Time-Resolved X-Ray Diffraction. *Phys. Rev. Lett.* **2017**, *118*, 247401.

(21) Haupt, K. Ultrafast Metamorphosis of a Complex Charge-Density Wave. *Phys. Rev. Lett.* **2016**, *116*, 016402.

(22) Tsen, A. W.; et al. Structure and control of charge density waves in two-dimensional 1T-TaS_2. *Proc. Natl. Acad. Sci. U. S. A.* **2015**, *112*, 15054−15059.

(23) Liu, G.; Rumyantsev, S.; Bloodgood, M. A.; Salguero, T. T.; Balandin, A. A. Low-Frequency Current Fluctuations and Sliding of the Charge Density Waves in Two-Dimensional Materials. *Nano Lett.* **2018**, *18*, 3630−3636.

(24) Geremew, A. K.; et al. Bias-Voltage Driven Switching of the Charge-Density-Wave and Normal Metallic Phases in 1T-TaS_2 Thin-Film Devices. *ACS Nano* **2019**, *13*, 7231−7240.

(25) Zhang, J.; et al. Photoexcitation Induced Quantum Dynamics of Charge Density Wave and Emergence of a Collective Mode in 1*T*-TaS_2. *Nano Lett.* **2019**, *19*, 6027−6034.

(26) Zhu, C.; et al. Light-Tunable 1T-TaS_2 Charge-Density-Wave Oscillators. *ACS Nano* **2018**, *12*, 11203−11210.

(27) Rajteri, M.; Taralli, E.; Portesi, C.; Monticone, E.; Beyer, J. Photon-number discriminating superconducting transition-edge sensors. *Metrologia* **2009**, *46*, S283−S287.

(28) Miller, A. J.; Nam, S. W.; Martinis, J. M.; Sergienko, A. V. Demonstration of a low-noise near-infrared photon counter with multiphoton discrimination. *Appl. Phys. Lett.* **2003**, *83*, 791−793.

(29) Lita, A. E.; Miller, A. J.; Nam, S. W. Counting near-infrared single-photons with 95% efficiency. *Opt. Express* **2008**, *16*, 3032.

(30) Chen, C.; Zhou, Z. Optical phonons assisted infrared absorption in VO_2 based bolometer. *Appl. Phys. Lett.* **2007**, *91*, No. 011107.
(31) Ma, H.; et al. Infrared micro-detectors with high sensitivity and high response speed using VO_2 -coated helical carbon nanocoils. *J. Mater. Chem. C* **2019**, *7*, 12095−12103.
(32) Zheng, S.; Liu, F.; Zhu, C.; Liu, Z.; Fan, H. J. Room-temperature electrically driven phase transition of two-dimensional 1T-TaS_2 layers. *Nanoscale* **2017**, *9*, 2436−2441.
(33) Wilson, J. A.; Di Salvo, F. J.; Mahajan, S. Charge-density waves and superlattices in the metallic layered transition metal dichalcogenides. *Adv. Phys.* **2001**, *50*, 1171−1248.
(34) Thomson, R. E.; Burk, B.; Zettl, A.; Clarke, J. Scanning tunneling microscopy of the charge-density-wave structure in 1*T*-TaS_2. *Phys. Rev. B: Condens. Matter Mater. Phys.* **1994**, *49*, 16899−16916.
(35) Perfetti, L. Time Evolution of the Electronic Structure of 1T-TaS_2 through the Insulator-Metal Transition. *Phys. Rev. Lett.* **2006**, *97*, 067402.
(36) Perfetti, L.; et al. Femtosecond dynamics of electronic states in the Mott insulator 1T-TaS_2 by time resolved photoelectron spectroscopy. *New J. Phys.* **2008**, *10*, No. 053019.
(37) Driscoll, T. Current oscillations in vanadium dioxide: Evidence for electrically triggered percolation avalanches. *Phys. Rev. B: Condens. Matter Mater. Phys.* **2012**, *86*, 094203.
(38) Stoliar, P.; et al. Universal Electric-Field-Driven Resistive Transition in Narrow-Gap Mott Insulators. *Adv. Mater.* **2013**, *25*, 3222−3226.

https://dx.doi.org/10.1021/acs.nanolett.0c02613
Nano Lett. 2020, 20, 6725−6731